Pertussis Toxin: Transition State Analysis for ADP-Ribosylation of G-Protein Peptide α_{i3}C20†

Johannes Scheuring and Vern L. Schramm*

Department of Biochemistry, Albert Einstein College of Medicine, 1300 Morris Park Avenue, Bronx, New York 10461

Received February 19, 1997; Revised Manuscript Received April 24, 1997⊗

ABSTRACT: Pertussis toxin from *Bordetella pertussis* is one of the ADP-ribosylating toxins which are the cytotoxic agents of several infectious diseases. Transition state analogues of these enzymes are expected to be potent inhibitors and may be useful in therapy. Pertussis toxin catalyzes the ADP-ribosylation of a cysteine in the synthetic peptide α_{i3}C20, corresponding to the C-terminal 20 amino acids of the α-subunits of the G-protein G_{i3}. A family of kinetic isotope effects was determined for the ADP-ribosylation reaction, using ^{3}H-, ^{14}C- and ^{15}N-labeled NAD^+ as substrates. Primary kinetic isotope effects were 1.050 ± 0.006 for [$1'_N$-^{14}C] and 1.021 ± 0.002 for [1_N-^{15}N], the double primary effect of [$1'_N$-^{14}C,1_N-^{15}N] was 1.064 ± 0.002. Secondary kinetic isotope effects were 1.208 ± 0.014 for [$1'_N$-^{3}H], 1.104 ± 0.010 for [$2'_N$-^{3}H], 0.989 ± 0.001 for [$4'_N$-^{3}H], and 1.014 ± 0.002 for [$5'_N$-^{3}H]. Isotope trapping experiments yielded a commitment factor of 0.01, demonstrating that the observed isotope effects are near intrinsic. Solvent D_2O kinetic isotope effects are inverse, consistent with deprotonation of the attacking Cys prior to transition state formation. The transition state structure was determined by a normal mode bond vibrational analysis. The transition state is characterized by a nicotinamide leaving group bond order of 0.14, corresponding to a bond length of 2.06 Å. The incoming thiolate nucleophile has a bond order of 0.11, corresponding to 2.47 Å. The ribose ring has strong oxocarbenium ion character. Pertussis toxin also catalyzes the slow hydrolysis of NAD^+ in the absence of peptides. Comparison of the transition states for NAD^+ hydrolysis and for ADP-ribosylation of peptide α_{i3}C20 indicates that the sulfur nucleophile from the peptide Cys participates more actively as a nucleophile in the reaction than does water in the hydrolytic reaction. Participation of the thiolate anion at the transition state provides partial neutralization of the cationic charge which normally develops at the transition states of *N*-ribohydrolases and transferases. Thus, the presence of the peptide provides increased S_N2 character in a loose transition state which retains oxocarbenium character in the ribose.

Bacterial ADP[1]-ribosylating toxins include pertussis, cholera, and diphtheria toxins and are involved in the pathochemistry of infectious diseases, causing thousands of deaths worldwide every year. New therapies against these diseases are required. The challenge is to develop specific and potent inhibitory agents, using the bacterial toxins as targets. Because of their high affinity to their cognate enzymes, transition state analogues are proposed to be powerful inhibitors (Wolfenden, 1972). Spectroscopic or structural analysis of stable complexes cannot provide the actual structure of the unstable and transient enzymatic transition states. However, the evaluation of kinetic isotope effect data can be used to reconstruct enzymatic transition state structure (Rodgers et al., 1982; Northrop, 1981). Catalysis must be the rate-limiting step in this approach, or appropriate conditions must be selected to make it rate limiting (Cleland, 1995). Determination of primary and secondary kinetic isotope effects around the reaction center, followed by a bond-energy bond-order normal mode analysis (Sims & Lewis, 1984), has been used with success for several enzymatic reactions (Schramm et al., 1994). The transition states of several different *N*-ribohydrolases have been determined by this method in recent years (Mentch et al., 1987; Parkin et al., 1991; Horenstein et al., 1991; Kline & Schramm, 1993, 1995; Rising & Schramm, 1997).

The catalytic action of the bacterial toxins is the ADP-ribosylation of specific amino acid side chains in different target proteins using NAD^+ as the substrate (Domenghini et al., 1995; Moss & Vaughan, 1985). The toxins catalyze the cleavage of the C−N bond between the anomeric C_N1' carbon of ribose and the nicotinamide nitrogen and transfer the ADP-ribosyl moiety to an acceptor molecule. Target proteins are the eukaryotic elongation factor eEF2 for diphtheria toxin (Van Ness et al., 1980) and G inhibitory or stimulatory proteins, which are involved in cell signal transduction, in the cases of the pertussis and cholera toxins (Gilman, 1987). ADP-ribosylation of the G-proteins prevents the coupling to their specific receptor proteins and consequently disrupts the signal transduction cascade (Katada et al., 1995; Ui, 1984). Besides their function as ADP-ribosyl transferases, the toxins also have NAD^+ glycohydrolase activity in the absence of an acceptor molecule (Katada et al., 1983). However, no physiological function is known for the hydrolysis reaction catalyzed by the toxins.

† This work was supported by NIH Research Grant AI34342.

* Corresponding author: telephone, (718) 430-2813; FAX, (718) 430-8565; email, vern@aecom.yu.edu.

⊗ Abstract published in *Advance ACS Abstracts,* June 15, 1997.

[1] Abbreviations: KIE, kinetic isotope effect; NAD^+, nicotinamide adenine dinucleotide, oxidized form; NMN, nicotinamide mononucleotide; ADP, adenosine diphosphate; DTT, dithiothreitol; TCA, trichloroacetic acid. The position of isotopic labels is indicated by subscripts N for the NMN portion of NAD^+ and A for the AMP portion of NAD^+. These are illustrated in Figure 1.

S0006-2960(97)00379-6 CCC: $14.00

G-proteins are heterotrimers, consisting of the α-subunits with the GTPase activity and β- and γ-subunits. Acceptors for ADP-ribosylation catalyzed by pertussis toxin are the α-subunits of G_i, G_O, and G_T. A cysteine residue four amino acids from the C-terminus is the acceptor for ADP-ribosylation (Katada & Ui, 1982; West et al., 1985). However, isolated α-subunits are reported to be weak substrates, and at least catalytical amounts of β- and γ-subunits are required for significant ADP-ribosylation (Casey et al., 1989). Attempts have been made to study the ADP-ribose transfer reaction using low molecular weight thiols like cysteine or dithiothreitol as model acceptors, but no ADP-ribosylation was detected in theses cases (McDonald et al., 1992). This is in contrast to the behavior of cholera toxin, where arginine and other guanidine compounds have been used as ADP-ribosyl acceptors for mechanistic studies (Moss & Vaughan, 1977; Oppenheimer, 1978). A synthetic peptide, corresponding to the last 20 amino acids of the G_{i3} α-subunit, has been found to be an acceptor for the ADP-ribosylation catalyzed by pertussis toxin (Graf et al., 1992) and has been used as a model substrate in kinetic and mechanistic studies (Finck-Barbancon & Barbieri, 1995; Scheuring & Schramm, 1995).

The mechanisms of the NAD^+ glycohydrolase activity of cholera and pertussis toxins have been studied by kinetic isotope effects, and the transition state structures have been proposed using the bond-energy bond-order vibrational analysis method (Sims & Lewis, 1984). The hydrolytic transition states are characterized by nearly dissociated nicotinamide groups and only insignificant interaction to the incoming water nucleophile. The ribose rings have an oxocarbenium ion structure, stabilized by delocalization of the positive charge of the leaving group and hyperconjugation between the C1′−C2′ and C1′−O4′ atoms (Rising & Schramm, 1997; Scheuring & Schramm, 1997). However, NAD^+ hydrolysis catalyzed by the bacterial toxins is not part of the normal toxin function. The synthetic peptide α_{i3}C20 permits the study of ADP-ribosyl transfer to a cysteine residue by pertussis toxin. Comparison with NAD^+ hydrolysis will establish if the presence of the peptide−Cys nucleophile causes a change in the nature of the transition state. In this study, we determined kinetic isotope effects from specifically labeled NAD^+, the catalytically active A-protomer of pertussis toxin, and an acceptor peptide from $G_{\alpha i3}$. The transition state structure was determined from the kinetic isotope effects using BEBOVIB calculations (Sims et al., 1977; Sims & Lewis, 1984).

MATERIALS AND METHODS

Materials. Pertussis toxin A protomer was purchased from List Biological Laboratories. NAD^+ was synthesized with specific ^3H, ^{14}C, and ^{15}N labels by published methods (Figure 1; Rising & Schramm, 1994). [8_A-^{14}C]NAD^+ was prepared using NMN, [8-^{14}C]ATP, and NAD^+ pyrophosphorylase. The peptide α_{i3}C20 was synthesized by solid-phase methods and the structure VFDRVTDVIIKNNLKECGLY confirmed by electrospray ionization mass spectrometry.[2]

[2] The authors thank Dr. Ruth H. Angeletti and Mr. Edward Nieves in the Laboratory for Macromolecular Analysis of the Albert Einstein College of Medicine. Mass 2253 was confirmed for the α_{i3}C20 peptide (Scheuring & Schramm, 1995).

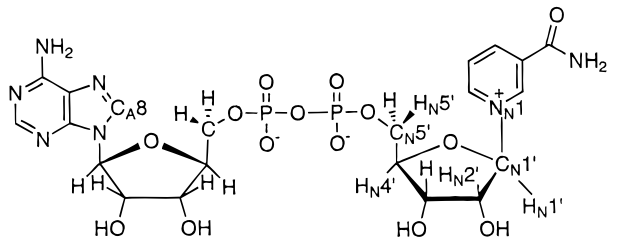

FIGURE 1: Structure of NAD^+ indicating positions in the molecule which were labeled with ^3H, ^{14}C, or ^{15}N, respectively, for kinetic isotope effects. The subscript N refers to the NMN portion of the molecule and subscript A to the adenylate portion of the molecule.

Kinetic Studies on ADP-Ribosylation. Samples containing 3 μg/mL pertussis toxin in 100 mM Tris-HCl and 20 mM DTT, pH 7.5, were incubated for 30 min at room temperature to activate the toxin. Peptide substrate was added, and the sample was incubated for another 10 min at 4 °C. The reaction was started by addition of NAD^+. Substrate concentrations were between 10 and 500 μM for the peptide and 10 and 350 μM for NAD^+. Samples with variable NAD^+ concentrations contained 500 μM peptide, and samples with variable peptide contained 250 μM NAD^+. Reaction mixtures contained 2×10^4 cpm [8_A-^{14}C]NAD^+ which was adjusted with unlabeled substrate to yield the desired concentrations. Samples were retrieved at 30 min intervals and analyzed on DEAE-Sephadex columns. NAD^+ eluted in 6 mL of 150 mM ammonium carbonate, pH 8.0, and the ADP-ribosylated peptide eluted in 4.5 mL of 1 M ammonium carbonate. Fractions of 1.5 mL were collected and analyzed by scintillation counting.

Product inhibition with ADP-ribosylated α_{i3}C20 peptide was investigated in steady-state kinetic conditions. The ADP-ribosylated peptide α_{i3}C20 was prepared as described recently (Scheuring & Schramm, 1995). Reaction mixtures of 50 μL contained 2.5 μg/mL pertussis toxin, 40 μM NAD^+ including 10^4 cpm [8_A-^{14}C]NAD^+, 70 μM peptide α_{i3}C20, and concentrations of the ADP-ribosylated peptide in the range of 50−300 μM in 50 mM phosphate, pH 7.5, and 20 mM DTT. Assays and analysis were performed as described above.

Commitment to Catalysis. Kinetic isotope effects can be interpreted into transition state structure only when the effects report directly on the chemical step(s) of the reaction. In irreversible reactions such as ADP-ribosylations, the most common feature which obscures isotope effects is irreversible binding of the labeled substrate to the enzyme. This is the commitment to catalysis problem (Northrop, 1981). To quantitate the commitment to catalysis, isotope trapping experiments were performed (Rose, 1980; Kline & Schramm, 1993). Samples of 10 μL containing 20 μM pertussis toxin and 200 μM NAD^+ including 7×10^4 cpm [8_A-^{14}C]NAD^+ were incubated for 15 s at 4 °C to form the binary Michaelis complex. The samples were then diluted with 100 μL of 10 mM NAD^+ containing variable concentrations of the peptide. Peptide concentrations from 50 to 500 μM were used to permit extrapolation to saturating peptide concentration. The sample was incubated to allow 5 to 10 turnovers followed by rapid analysis using DEAE-Sephadex anion-exchange chromatography on 1 mL columns. Control experiments for formation of labeled product during the incubation steps contained the identical amounts of enzyme and labeled substrates as used in the trapping experiments

to quantitate NAD^+ hydrolysis rates. Substrate NAD^+ and ADP-ribosylated peptide were collected from DEAE columns as described above and analyzed for the formation of labeled product by scintillation counting.

Solvent Isotope Effect. Reaction mixtures with 200 μM NAD^+ and peptide α_{i3}C20 concentrations of between 70 and 500 μM were made with a variable D_2O content between 0% and 65%. Reaction rates were measured at 4 °C where transfer of ADP-ribose to peptide α_{i3}C20 is quantitative. Samples were taken at 30 min intervals and analyzed as described above.

Measurement of Kinetic Isotope Effects. NAD^+ samples containing approximately 10^5 cpm each of the substrates labeled in the sensitive and in the remote positions were adjusted with unlabeled NAD^+ to give a final concentration of 100 μM in the sample. The mixture was purified on a Nucleosil RP18 HPLC column (7.9 × 300 mm) with an eluent of 50 mM ammonium acetate, pH 5.0, and lyophilized.

Two identical reaction mixtures were prepared; one reaction was taken to 20−40% completion and the other was converted completely to products. Samples of 300 μL for the 20−40% ADP-ribosylation reaction contained 1 μg of pertussis toxin A protomer in 50 mM potassium phosphate, pH 7.5, 20 mM DTT, and 1% BSA. Complete reaction mixtures contained 2 μg of pertussis toxin in the same buffer. The mixtures were incubated for 30 min at room temperature to activate the toxin. The reaction was started by addition of the peptide to a final concentration of 500 μM, followed by the NAD^+, and the samples were incubated for 4 h or until complete conversion was achieved at 4 °C. The product, ADP-ribosylated peptide, and the remaining NAD^+ substrate were separated on 1 mL DEAE-Sephadex anion-exchange columns. Unreacted NAD^+ was eluted with 6 mL of 150 mM ammonium bicarbonate, pH 8.0, and ADP-ribosylated peptide was eluted with 5 mL of 1 M ammonium bicarbonate. Fractions of 1 mL were collected.

In an alternative method, 60 μL portions of the reaction mixture were added to 120 μL of an ice-cold solution containing 1 mM unlabeled NAD^+ and 0.5 mM peptide and were precipitated by adding 200 μL of ice-cold 30% TCA solution. The precipitates were washed with 500 μL of 5% TCA solution and 2 × 500 μL of diethyl ether and dissolved in 500 μL of 200 mM Tris-HCl, pH 8.0, and 5% SDS. To control for quenching effects, peptide treated in the same way as the samples was added to the ^{14}C-standard vial. The ^{3}H/^{14}C ratio of the 30% and the complete reactions was determined by scintillation counting. The samples of each experiment were analyzed for at least 10 counting cycles of 10 min per sample. The resulting KIE's were calculated from ^{3}H and ^{14}C standards and the ^{3}H/^{14}C ratios from the 20−40% and 100% reactions.

Transition State Modeling. The transition state structure consistent with the experimentally determined kinetic isotope effects was calculated using the BEBOVIB program (Sims et al., 1977). This approach locates the transition state by using normal mode analysis to compare the vibrational energy of substrate and transition state for normal and isotopically labeled molecules, and thus the predicted isotope effects. Thus, a systematic prediction of KIE for various transition state structures was used to locate the transition state bonding pattern which gives rise to the experimental KIE. Coordinates for the ground state structure of NAD^+ were taken from the crystal structure of NAD^+ bound to diphtheria toxin (Bell & Eisenberg, 1996; data from Brookhaven National Laboratory Protein Data Bank, 1TOX). The geometry of the NMN portion of the molecule was optimized by MOPAC 6.0 calculations using the PM3 basis set (Merz & Besler, 1990), freezing two dihedral angles in the ribose ring to maintain the 3′-endo conformation known to dominate the solution and crystal structure. This was necessary since the PM3 semiempirical method otherwise flattens the ribosyl ring to a conformation not observed in actual structures. Coordinates for an oxocarbenium transition state are based on the ribonolactone crystal structure as the starting ring geometry (Kinoshita et al., 1981). The carbonyl oxygen was replaced by a hydrogen atom, and the structure converted to the transition state by including a positive charge in the ribosyl ring. The structure was then minimized using the PM3 basis set in MOPAC. The incoming nucleophile was included in the transition state model as a single sulfur atom. Since the C1′−S bond order is low relative to a covalent bond, the calculated KIE's were insensitive to replacement of the single sulfur atom by CH_3SH or CH_3S^-. Standard bond length, stretching, and angle bend force constants were taken from Cornell et al. (1995). These are also used in the AMBER algorithm and represent more extensive bond parameters than originally provided in the BEBOVIB suite. Use of the improved parameters makes a small but significant change in the analysis of the transition state structure (Scheuring & Schramm, 1997). The model was adjusted to fit the experimental KIE's as described (Rising & Schramm, 1997) by systematic variation of C1′−N1, C1′−O4′, C1′−C2′, C1′−H1′, C2′−H2′, and C1′−O bond orders and associated bond angles.

RESULTS

Kinetic Constants for Substrates and Products. Pertussis toxin catalyzes ADP-ribosylation of the peptide α_{i3}C20 at temperatures between 4 and 20 °C (Finck-Barbancon & Barbieri, 1995; Scheuring & Schramm, 1995). Higher temperatures cause precipitation of the peptide and the toxin. At 20 °C pertussis toxin catalyzed both the ADP-ribosylation of the peptide and some NAD^+ hydrolysis. The simultaneous hydrolytic and transfer reactions complicate interpretation of the observed kinetic isotope effects. At 4 °C, the k_{cat} for NAD^+ hydrolysis was only 0.024 min^{-1}, whereas the k_{cat} of ADP-ribosylation was 3.0 min^{-1}. This rate of NAD^+ hydrolysis is negligible and does not interfere with the kinetic isotope effects of the ADP-ribosylation reaction. Apparent K_m values of 69 and 27 μM were found for the peptide and for NAD^+ for the transferase reaction at 4 °C. K_m values reported in the literature are 11 or 50 μM for the peptide and 2 or 14 μM for NAD^+ (Graf et al., 1992; Finck-Barbancon & Barbieri, 1995).

Kinetic studies in the presence of the product ADP-ribosyl-α_{i3}C20 in concentrations between 50 and 300 μM resulted in weak product inhibition with fixed substrate concentrations near the K_m values. The apparent K_i value for the product is 150 μM. The product therefore has a lower apparent affinity to the toxin than either the peptide substrate or NAD^+. The relatively poor binding of the ADP-ribosyl

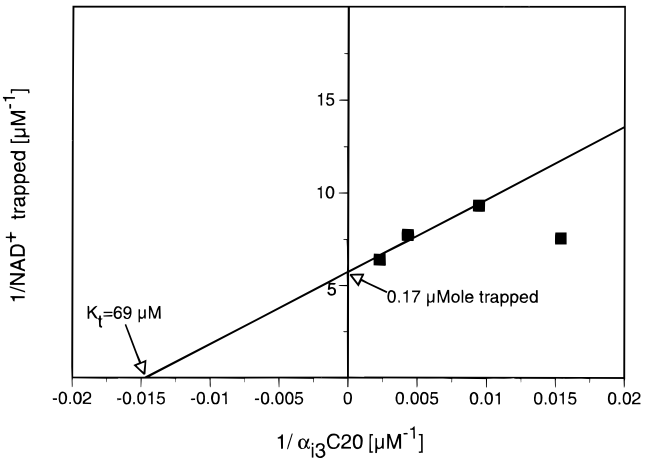

FIGURE 2: Commitment to catalysis for the ADP-ribosylation of peptide α_{i3}C20 by pertussis toxin. Pertussis toxin was present at 20 μM and [8_A-^{14}C]NAD$^+$ at 200 μM in a volume of 10 μL for the first 15 s. The mixture was diluted to 100 μL with the indicated concentration of peptide α_{i3}C20 containing 10 mM unlabeled NAD$^+$. After 1.5 min, the reaction was stopped and the amount of labeled ADP-ribosyl peptide was analyzed. This is indicated as "NAD$^+$ trapped" on the ordinate. The apparent affinity constant K_t is the concentration of α_{i3}C20 that causes half-maximal trapping. Thus K_t is analogous to the K_m for this substrate in a steady-state analysis (Rose, 1980).

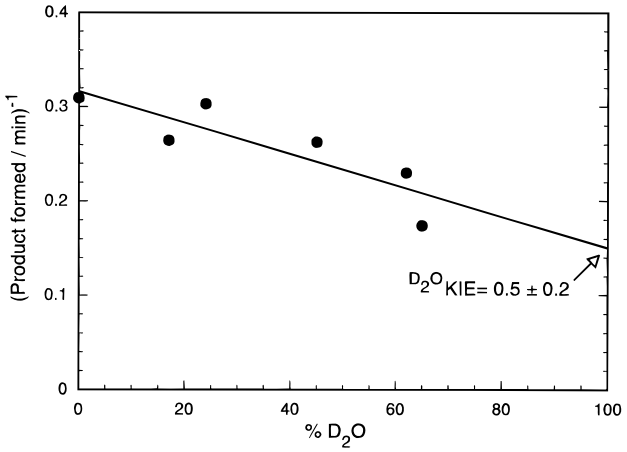

FIGURE 3: Solvent D_2O kinetic isotope effect for the formation of ADP-ribosyl-α_{i3}C20 by pertussis toxin. In this experiment, the reaction mixtures contained 200 μM NAD$^+$ and 500 μM peptide α_{i3}C20. These conditions result in initial reaction rates near V_{max}. The line was fit to the experimental data by a linear least squares analysis. The value ^{D_2O}KIE is the observed solvent isotope effect extrapolated to 100% D_2O.

peptide contributes to catalytic efficiency since weak binding is associated with rapid release rates.

Commitment to Catalysis. A small fraction of toxin-bound NAD$^+$ is converted to product ADP-ribosylated-α_{i3}C20 as a function of peptide concentration in the commitment to catalysis experiment. Extrapolation to saturating peptide concentration results in a forward commitment factor of 0.01 (Figure 2). A commitment factor of this magnitude is well below the experimental error in kinetic isotope effect measurements and does not influence the kinetic isotope effects in a significant way. The measured KIE's are therefore experimentally intrinsic and can be used to interpret transition state structure.

Solvent Isotope Effect. Initial reaction rates of samples with variable D_2O content were determined at 4 °C under saturating substrate concentrations. The reciprocal plot of these data is shown in Figure 3, indicating an inverse solvent isotope effect. Extrapolation to 100% D_2O resulted in an estimated solvent isotope effect of 0.52 ± 0.18. Experiments with peptide concentrations fixed near the K_m value (70 μM) resulted in the same inverse solvent isotope effect of 0.5. The solvent isotope effects were also measured at room temperature, with a similar result of 0.47 ± 0.14. Deprotonation of a cysteine sulfhydryl group in the presence of D_2O is expected to result in an inverse solvent isotope effect (Quinn & Sutton, 1991; Weiss et al., 1987). The observed solvent isotope effect could therefore be due to the deprotonation of the nucleophilic thiol group, suggesting that cysteine ionization occurs prior to transition state formation. Smaller inverse isotope effects between 0.73 and 0.82 have been observed for NAD$^+$ hydrolysis catalyzed by pertussis and cholera toxins (Rising & Schramm, 1997; Scheuring & Schramm, 1997).

Kinetic Isotope Effects. A family of primary and secondary KIE's was measured for NAD$^+$ labeled in the sensitive NMN moiety positions [$1'_N$-^{14}C], [1_N-^{15}N,$5'_N$-^{14}C], [1_N-^{15}N,$1'_N$-^{14}C], [$1'_N$-^{3}H], [$2'_N$-^{3}H], [$4'_N$-^{3}H] and [[$5'_N$-^{3}H] (Figure 1). Remote labels were [$5'_N$-^{14}C]- or [8_A-^{14}C]NAD$^+$ for the measurement of ^{3}H KIE's and [$4'_N$-^{3}H]NAD$^+$ for ^{14}C KIE's. The experimental results are summarized in Table 1. Two independent methods were used to separate the products and substrate for isotopic ratio measurement. In most experiments, separation of NAD$^+$ from ADP-ribosyl-α_{i3}C20 was performed on DEAE-Sephadex columns. Acid precipitation of ADP-ribosylated peptide was used in independent experiments. The data from both methods gave equivalent kinetic isotope effects. The second method is more efficient since the substrate and products are collected in single fractions. Both the statistical analysis and the scintillation counting procedures for double-labeled samples are simplified for single sample analysis.

A relatively large primary [$1'_N$-^{14}C] KIE of 1.050 ± 0.006 was found for ADP-ribosylation of peptide α_{i3}C20. A large primary [$1'_N$-^{14}C] KIE indicates significant participation of the attacking thiol nucleophile at the transition state. The small primary [1_N-^{15}N] KIE indicates substantial but less than full dissociation of the nicotinamide leaving group. The double primary KIE of 1.064 ± 0.002 is within experimental error of 1.072 ± 0.008 predicted from the values of the single primary KIE's.

The α-secondary kinetic isotope effect from [$1'_N$-^{3}H]NAD$^+$ is 1.208 ± 0.014 and the β-secondary isotope effect is 1.104 ± 0.010. Large α-secondary isotope effects are primarily a result of out of plane bending motion for the 1′-proton. The source of β-secondary isotope effects at the $2'_N$-H position is hyperconjugation at the C1′−C2′ bond. Both isotope effects are characteristic of an oxocarbenium ion character for the ribose ring at the transition state.

In the remote positions, KIE's of 0.989 ± 0.001 for [$4'_N$-^{3}H]NAD$^+$ and 1.014 ± 0.002 for [$5'_N$-^{3}H]NAD$^+$ were measured. Similar KIE's in these positions have been found for other *N*-ribohydrolases, including the NAD$^+$ hydrolysis catalyzed by pertussis toxin (Scheuring & Schramm, 1997). Remote isotope effects are the consequence of ribosyl ring distortion during enzymatic catalysis, since they do not occur in the pH-independent chemical hydrolysis of NAD$^+$ (Rising & Schramm, 1997).

Table 1: Kinetic Isotope Effects for ADP-Ribosylation of Peptide α_{i3}C20 and NAD^+ Hydrolysis by Pertussis Toxin

substrates	sensitive isotopic label	KIE	
		ADP-ribosylation	NAD^+ hydrolysis[d]
[1′-^{14}C]- and [4′-^{3}H]NAD^+	[1′-^{14}C], primary[a]	1.050 ± 0.006 (6)[c]	1.021 ± 0.001
[1-^{15}N]- and [4′-^{3}H]NAD^+	[1-^{15}N,5′-^{14}C], primary[a]	1.021 ± 0.002 (7)	1.021 ± 0.004
[1-^{15}N, 1′-^{14}C]- and [4′-^{3}H]NAD^+	[1-^{15}N,1′-^{14}C], double primary[a]	1.064 ± 0.002 (3)	1.049 ± 0.004
[1′-^{3}H]- and [5′-^{14}C]NAD^+ [b]	[1′-^{3}H], α-secondary	1.208 ± 0.014 (6)	1.211 ± 0.010
[2′-^{3}H]- and [5′-^{14}C]NAD^+ [b]	[2′-^{3}H], *β*-secondary	1.104 ± 0.010 (4)	1.144 ± 0.005
[4′-^{3}H]- and [5′-^{14}C]NAD^+ [b]	[4′-^{3}H], *γ*-secondary	0.989 ± 0.001 (3)	0.989 ± 0.001
[5′-^{3}H]- and [5′-^{14}C]NAD^+	[5′-^{3}H], *δ*-secondary	1.014 ± 0.002 (3)	1.019 ± 0.004

[a] Observed isotope effects were corrected by the formula (obs KIE × [4′-^{3}H]KIE). [b] In some experiments [8_A-^{14}C]NAD^+ was used as the remote label. Results were in agreement with those using [5′-^{14}C]NAD^+, and the average KIE's shown here include data using both remote labels. [c] Number of experiments. [d] The KIE for NAD^+ hydrolysis are from Scheuring and Schramm (1997).

Table 2: Kinetic Isotope Effects from [1′$_N$-^{3}H]NAD^+ for the ADP-Ribosylation of the Peptide α_{i3}C20 by Pertussis Toxin Are pH Independent

pH	KIE	k_{cat} (min^{-1})
6.0	1.215 ± 0.008	1.6
7.0	1.213 ± 0.015	2.8
7.5	1.208 ± 0.014	3.0
8.0	1.220 ± 0.013	3.0
9.0	1.222 ± 0.007	3.7

The [1′$_N$-^{3}H] KIE was measured over the pH range from 6.0 to 9.0. No change in kinetic isotope effects was observed as a function of pH. The kinetic isotope effects were constant near 1.21 (Table 2). This pH-independent behavior of kinetic isotope effects was also found for NAD^+ hydrolysis catalyzed by pertussis toxin (Scheuring & Schramm, 1997).

Transition State Modeling. On the basis of the conformation of NAD^+ bound to diphtheria toxin, a reactant state substrate structure was established for the NMN moiety (Figure 4, top). The starting structure for the ribose ring at the transition state was taken from crystallographic data of ribonolactone (Kinoshita et al., 1981). Ribonolactone has an sp^2-hybridized anomeric carbon atom, and the structure is therefore similar to the deduced oxocarbenium ion structure of the transition state. The exocyclic lactone oxygen was replaced by a hydrogen atom, to approximate the transition state. Both structures were minimized by MOPAC PM3 calculations. Constraints in two dihedral angles of the ribose ring were made to keep a 3′-endo ring configuration for the substrate and a 3′-exo conformation for the transition state because of the tendency for MOPAC PM3 to flatten ribosyl rings. A cutoff model of the pyrimidine ring, containing the N1, C2, C3, C5, C6, H2, and H6 atoms, was added to the optimized ribonolactone structure. The incoming nucleophile was modeled as a single sulfur atom. Additional atoms attached to the sulfur nucleophile (e.g., a carbon atom) gave no change in the calculated kinetic isotope effects for a fixed transition state geometry.

The experimental kinetic isotope effects could be matched to a transition state structure with ribooxocarbenium character which included partial bonds to both nicotinamide and cysteineyl peptide. Transition state structures with leaving group bond orders between 0.13 and 0.14 and bond orders to the incoming nucleophile between 0.05 and 0.11 are consistent with the experimental kinetic isotope effects. Higher bond orders to either or both leaving group and nucleophile required an increase in the total bond order at the anomeric C1′ atom to match the experimental KIE.[3] Keeping the total bond order to C1′ constant in reactant and transition state resulted in a transition state structure with 0.05 bond order to the sulfur and 0.13 to the nicotinamide group. Increasing the single bond stretching force constant for O4′−C1′ by 15% in the transition state resulted in a transition state with bond orders of 0.14 and 0.11 to leaving group and nucleophile, respectively (Figure 4, middle, and Table 3). Increased stretching force constants to C1′ at the transition state have been used to match the experimental kinetic isotope effects for NAD^+ hydrolysis by pertussis toxin (Scheuring & Schramm, 1997). Ab initio studies have indicated that the force constants in oxocarbenium ions can increase more rapidly than the linear function usually used in normal mode analysis such as BEBOVIB (Mentch et al., 1987).[4]

The small partial bond orders to the leaving group and attacking thiolate nucleophile cause the structure of the ribose ring to be oxocarbenium like. The partial positive charge is stabilized by delocalization into the C1′−O4′ bond. There is also hyperconjugation to the C1′−C2′ bond. About 6 % of the additional bond order from the C1′−O4′ bond is delocalized into the C1′−C2′ bond. This extent of bond delocalization is necessary to match the experimentally observed [2′$_N$-^{3}H] KIE of 1.104 ± 0.010. The C1′−O4′ bond of ribose has a nearly full double bond character in this transition state structure.

DISCUSSION

Summary. The transition state for the ADP-ribosylation of the peptide α_{i3}C20 by pertussis toxin is an asymmetric, concerted displacement reaction with a loose transition state. There is substantial bond order to both the leaving group and the ionized sulfur nucleophile at the transition state. However, the ribose ring has oxocarbenium ion character.

Intrinsic Kinetic Isotope Effects. Interpretation of competitive V_{max}/K_m kinetic isotope effects in terms of transition state structure requires that the isotope effects reflect the chemical step of the reaction and are not obscured by kinetic factors. The most common of these is forward commitment, the probability for NAD^+ bound to the toxin to be converted to product relative to release as free NAD^+. Isotope trapping experiments quantitate this ratio (Rose, 1980). Reverse commitment, the conversion of enzyme-bound products to substrates prior to product release, is unlikely for thiolysis

[3] Ab initio calculations using the conversion of a truncated region around C_N1' of NMN^+ to the oxocarbenium ion (Gaussian 94) confirmed that an increase in bond order at the reaction center can occur (Dr. Paul J. Berti, personal communication).

[4] Paul J. Berti and Vern L. Schramm, unpublished observations.

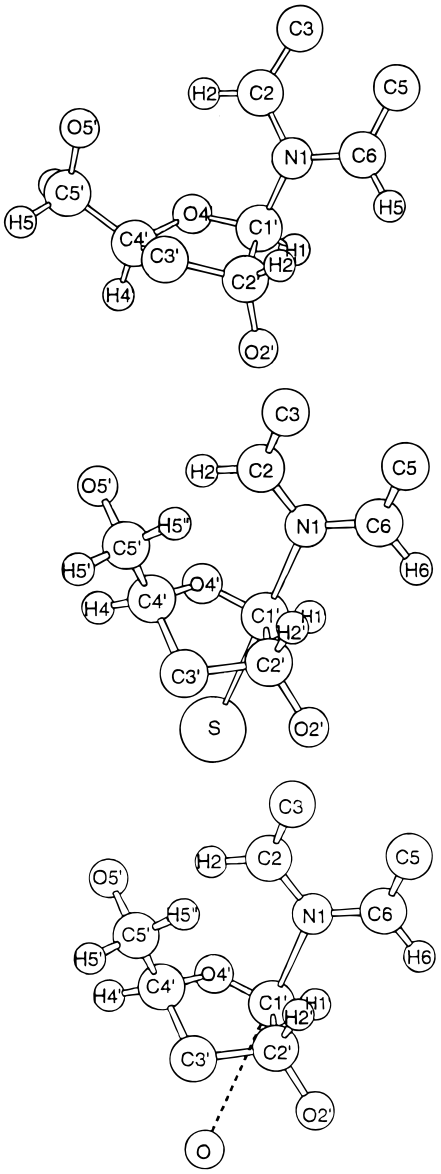

FIGURE 4: (Top) Abbreviated structure of the NMN portion of NAD^+ as used for the substrate in BEBOVIB calculations (Sims & Lewis, 1984). Only atoms used in the BEBOVIB file are shown. The torsion angle between the ribose and nicotinamide rings and the ribose pucker are based on NAD^+ bound to diphtheria toxin (Bell & Eisenberg, 1996). (Middle) The transition state structure for ADP-ribosylation of the peptide α_{i3}C20. Only the atoms used in BEBOVIB calculations are shown. The incoming nucleophile is represented by a sulfur atom. The model was calculated from BEBOVIB fitting to give bond angles and bond orders in the ribose ring which are consistent with all of the experimentally determined kinetic isotope effects. (Bottom) The transition state structure for NAD^+ hydrolysis catalyzed by pertussis toxin.

of the high-energy N-ribosidic bond (Rising & Schramm, 1997). The experimentally measured forward commitment of 0.01 at saturating peptide α_{i3}C20 and near-saturating NAD^+ establishes no significant forward commitment and indicates that the observed isotope effects are within experimental error of the intrinsic values. Intrinsic isotope effects are suitable for analysis of transition state structure.

Ionization of the Cysteine Nucleophile. The concerted attack of the peptide α_{i3}C20 is known to cause inversion of configuration at C1′ of ADP-ribose (Scheuring & Schramm, 1995). To be competent for attack, the sulfhydryl must ionize. Solvent isotope effects in D_2O would be predicted to give a large normal isotope effect if proton transfer from the sulfhydryl to the base is occurring at the transition state. If ionization occurs prior to transition state formation, an inverse isotope effect is predicted since in D_2O more of the sulfhydryl will be in the reactive, ionized form. The inverse solvent isotope effect of 0.5 confirms proton transfer prior to reaching the transition state.

Table 3: Bond Order and Bond Length for NAD^+ Reactant and Transition State Structures for ADP-Ribosylation of Peptide α_{i3}C20 and NAD^+ Hydrolysis by Pertussis Toxin A Protomer

			transition state structures for pertussis toxin			
	reactant structure NAD+		α_{i3}C20-ADP-ribosylation[a]		NAD^+ hydrolysis[b]	
bond	bond order	Å	bond order	Å	bond order	Å
C1′−N1	0.836	1.529	0.140	2.065	0.110	2.14
C1′−O4′	1.015	1.406	1.735	1.245	1.850	1.23
C1′−C2′	0.862	1.570	0.904	1.555	0.921	1.55
C1′−H1′	0.903	1.121	0.863	1.134	0.945	1.11
C2′−H2′	0.920	1.115	0.878	1.129	0.861	1.14
C1′−nucl	0	>3.5	0.110	2.472	<0.002	>3.5

[a] The transition state structure is in agreement with all of the intrinsic kinetic isotope effects predicted by bond-vibrational analysis (Sims et al., 1977). [b] Data for the transition state structure of NAD^+ hydrolysis by pertussis toxin are taken from Scheuring and Schramm (1997) and are included here for comparative purposes.

Nucleophilic Participation at the Transition State. The transition state for ADP-ribosylation of α_{i3}C20 differs from that of NAD^+ hydrolysis catalyzed by the same enzyme in the experimental value for the [1′$_N$-^{14}C] primary kinetic isotope effects. The relatively large [1′$_N$-^{14}C] kinetic isotope effect of 1.050 ± 0.006 for ADP-ribosylation is characteristic of significant nucleophilic participation in the transition state. The smaller KIE of 1.021 ± 0.004 indicated that there is no significant nucleophilic participation of the attacking water at the transition state of the NAD^+ hydrolysis reaction (Scheuring & Schramm, 1997). The [1$_N$-^{15}N] KIE and the resulting bond order of the nicotinamide leaving group and the ribose ring are similar for both NAD^+ hydrolysis and ADP-ribosylation of the peptide, indicating that the nucleophilicity resides in the attacking cysteine thiolate.

Structure of the Ribose Ring at the Transition State. The transition state for ADP-ribosyl transfer is oxocarbenium ion like and incorporates most of the positive charge associated with nicotinamide prior to reaction of the attacking thiolate nucleophile. Most of the bond order from the scissile C−N bond is stabilized within the ribooxocarbenium ion. The [2′$_N$-^{3}H] KIE of 1.104 for ADP-ribosyl transfer is less than that of 1.144 for NAD^+ hydrolysis and represents a slightly diminished extent of hyperconjugation as a consequence of the increased bond order from the attacking nucleophile. Other possibilities for the [2′$_N$-^{3}H] KIE have been discussed and are less consistent with data than the hyperconjugation explanation (Scheuring & Schramm, 1997). Hyperconjugation causes the C1′−O4′ and C1′−C2′ bonds to be somewhat longer at the transition state than those for the hydrolysis of NAD^+ by pertussis toxin (Scheuring & Schramm, 1997). The α-secondary ^{3}H kinetic isotope effect of 1.21 is near the upper limit which has been observed for solution solvolysis studies of NAD^+, NMN^+, and nicotinamide riboside. For example, values of 1.19 were determined for [1′$_N$-^{3}H]NAD^+ for both the pH-independent solvolysis and the cholera toxin catalyzed hydrolysis (Rising

& Schramm, 1997). The large [$1'_N$-^{3}H] isotope effect is surprising for the ADP-ribosylation reaction which occurs with significant participation of the attacking cysteinyl-peptide nucleophile. Small or inverse α-secondary ^{3}H kinetic isotope effects are predicted in symmetric S_N2 transition states due to steric restrictions on the out of plane bending of the 1′-proton (Melander & Saunders, 1980). However, it has been recognized that dissociated S_N2 transition states allow a higher degree of freedom to the proton, resulting in larger kinetic isotope effects (Poirier et al., 1994). In addition, α-secondary kinetic isotope effects from soft nucleophiles like sulfur are reported to be larger than the corresponding reactions with hard nucleophiles like oxygen (Melander & Saunders, 1980). These kinetic isotope effects correspond to a distance from C1′ to the nucleophile of 2.47 Å and that to the leaving group of 2.06 Å. The latter is approximately the same as in the hydrolysis by pertussis toxin where a [1′-^{3}H] KIE of 1.207 was found (Scheuring & Schramm, 1997). A bond length of more than 2 Å at the transition state allows sufficient space for out of plane bending freedom to explain this large α-secondary kinetic isotope effect.

Comparison of Transition States for ADP-Ribosylation and NAD$^+$ Hydrolysis by Pertussis Toxin. The transition state structure for ADP-ribosylation of peptide α_{i3}C20 is closely related to that for NAD$^+$ hydrolysis by pertussis toxin (Figure 4 and Table 3). In the reaction coordinate, the C1′−N1 bonds are similar at 2.065 and 2.14 Å for ADP-ribosylation and NAD$^+$ hydrolysis, respectively (Table 3). As the nicotinamide group leaves, the partial positive charge on the leaving group is neutralized as the bond is broken. The nearly equivalent bond orders to nicotinamide in the transition states of NAD$^+$ hydrolysis or ADP-ribosylation could be the result of fixed catalytic site distances between the regions which stabilize the nicotinamide and ribooxocarbenium portions of the transition state or could reflect the intrinsic chemical energy of the transition state structure. Computational analysis of nicotinamide *N*-ribosyl cleavage has also predicted oxocarbenium character at the transition state (Schröder et al., 1992).

The major difference between these transition states is stronger nucleophilic participation by the thiolate anion of peptide α_{i3}C20, giving a S−C1′ distance of 2.47 Å compared to a distance of >3.0 Å with water as the nucleophile. Attack by the thiolate anion creates a near-neutral transition state ensemble containing the closely separated ion pair of the oxocarbenium ion and the attacking thiolate. This effect is clearly evident in Figure 5, which shows the electrostatic potential surfaces of the transition states with and without participation of a CH_3S^- ion as a small atomic model for the ionized peptide. Transition states for solvolysis of NAD$^+$ or hydrolysis by pertussis and cholera toxins (Rising & Schramm, 1997; Scheuring & Schramm, 1997) have less nucleophilic participation, and in solution, the formation of a mixture of α and β anomers of ADP-ribose product suggests sufficient lifetime for the oxocarbenium ion to permit limited solvent competition for the ribosyl face from which nicotinamide departs (Oppenheimer & Tashma, 1992).

Nature of the α_{i3}C20 Peptide. The catalytic site specificity of pertussis toxin results in the ADP-ribosylation of a specific Cys located four amino acids from the C-terminus of G-proteins. Low-molecular-weight thiols including the tripeptide glutathione are not ADP-ribosylated by pertussis toxin at concentrations to 200 mM. A peptide of at least 10 amino acids is required for productive binding of the acceptor to the toxin. In addition, hydrophobic amino acids at the C-terminus and Cys at the fourth residue from the C-terminus are essential for successful ADP-ribosylation (Neer et al., 1988; Avigan et al., 1992). The peptide α_{i3}C20, corresponding to the last 20 C-terminal acids of the G-proteins $G\alpha_{i3}$, is

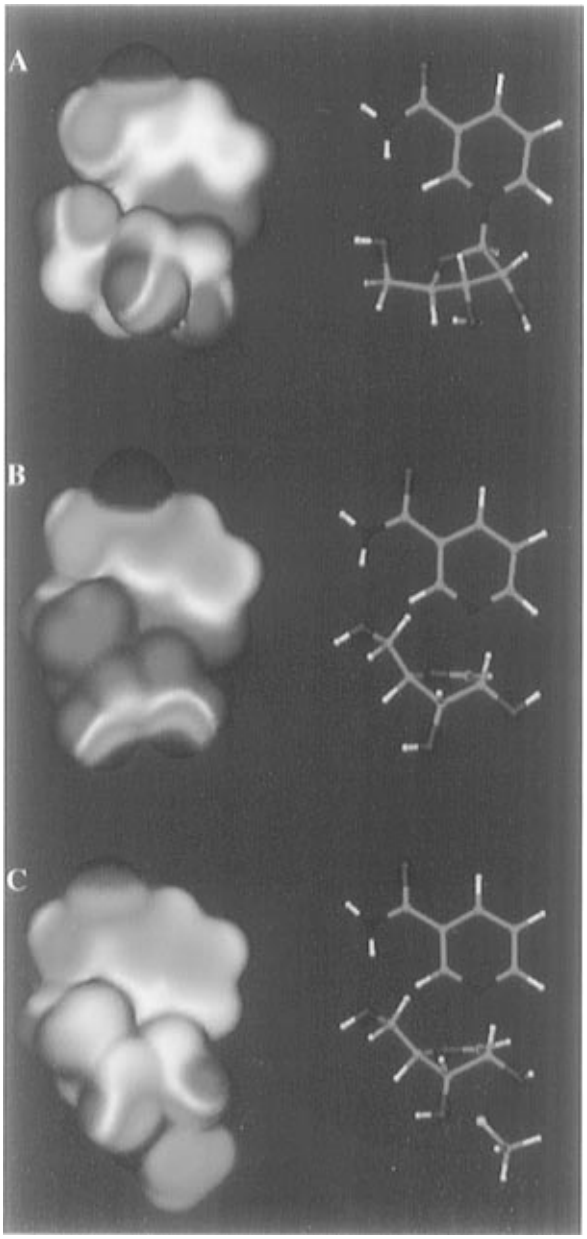

FIGURE 5: Electrostatic potentials at the molecular surfaces of reactant nicotinamide riboside (A), the transition state for the ADP-ribosylation reaction of pertussis toxin showing nicotinamide riboside with the attacking thiolate peptide removed (B), and the transition state nicotinamide riboside with participation of the nucleophilic thiolate anion (C). The electrostatic potentials on the left are presented at an electron density of 0.002 e/b^3 (Horenstein & Schramm, 1993). The view of the electrostatic potential surfaces is the same as for the corresponding stick figures on the right. The electron density and electrostatic potentials are calculated from the CUBE function of Gaussian 94. Visualization of the surfaces uses AVS Chemistry Viewer. Blue represents electron-rich regions and red indicates relative electron deficiencies. The corresponding stick figures were also created with the AVS package where green, red, yellow, blue and white represent carbon, oxygen, sulfur, nitrogen, and hydrogen. The geometry of the carboxamide was fixed at that proposed from the crystal structure (Bell & Eisenberg, 1996).

a suitable model compound to study the mechanism of ADP-ribosylation.

The G_{i1} α-subunits have a high similarity to G_{i3} α-subunits around the ADP-ribosylation site and have been characterized by X-ray crystallography (Coleman et al., 1994; Mixon et al., 1995). There are uncertainties in the structure of the C-terminal region, corresponding to the ADP-ribosylation sequence. In the presence of a GTP analogue, the last 10 amino acids are missing ordered electron density, indicating flexibility or multiple conformations (Coleman et al., 1994). The ordered part of the C-terminal protein structure is an α-helix. In contrast, in the presence of GDP the entire C-terminal region forms an α-helical motif, but Cys351 is not accessible for ADP-ribosylation in this structure (Mixon et al., 1995). Thus, one action of the GDP/GTP exchange appears to be a conformational change which exposes Cys351 for covalent modification. At the lower temperatures used in this study, the helix motif may be more ordered with the Cys exposed to provide the necessary contacts to the protein binding site on the toxin. GTP was not required for the ADP-ribosylation reaction observed here.

The kinetic isotope effects and the resulting transition state structure for ADP-ribosylation of the α_{i3}C20 peptide should be similar to that for the physiological reaction since ADP-ribosylation predominates. NAD^+ hydrolysis by pertussis toxin has no known physiological function and is only observed in the absence of competent acceptor molecules. In the ADP-ribosylation reaction, binding of the α_{i3}C20 peptide brings the thiol group of the cysteine in proximity to the C1′ anomeric carbon atom. This nucleophilic participation of the Cys residue and the stereochemistry of the reaction are consistent with a concerted mechanism with an expanded, loose S_N2-like transition state.

Implications for Transition State Inhibitor Design. The development of inhibitors can be focused toward attempts to mimic the NAD^+ portion of the transition state since hydrolysis occurs without acceptors. Elements of the thiolate nucleophile contribute an additional 2 orders of magnitude toward rate enhancement. The essential interactions between the peptide and the toxin extend beyond the nucleophilic Cys, based on the inability of pertussis toxin to ADP-ribosylate cysteine or other low-molecular-weight thiols. Introduction of other elements of the cysteine-containing peptide should permit modest enhancement of inhibition above that provided by an oxocarbenium analogue of NAD^+. It has been reported that "mutants" of this peptide which include a serine instead of the cysteine inhibited the ADP-ribosylation of several G-proteins and of the peptide α_{i3}C20 itself (Graf et al., 1992). However, the weak inhibition by ADP-ribosylated α_{i3}C20 indicates that electrostatic and geometric features of the transition state will be required for tight binding as a transition state analogue.

Phenyliminoribitol and phenylriboamidrazone and related derivatives have been shown to be powerful inhibitors for other *N*-ribohydrolases (Horenstein & Schramm, 1993; Boutellier et al., 1994). These compounds were designed as transition state analogues of a dissociated transition state with oxocarbenium character of the ribose ring. Incorporation of the features of these compounds into NAD^+ or ADP-ribosyl peptide analogues holds promise for potent inhibitors for pertussis and related ADP-ribosylating toxins.

ACKNOWLEDGMENT

The authors thank Dr. Paul J. Berti for his advice and for providing the spreadsheet program which calculates kinetic isotope effects from scintillation counting of multiple channel isotope detection. We thank Dr. Carey K. Bagdassarian for the preparation and printing of Figure 5.

REFERENCES

Avigan, J., Murtagh, J. J., Stevens, L. A., Angus, C. W., Moss, J., & Vaughan, M. (1992) *Biochemistry 31*, 7736−7740.
Bell, C. E., & Eisenberg, D. (1996) *Biochemistry 35*, 1137−1149.
Boutellier, M., Horenstein, B. A., Semenyaka, A., Schramm, V. L., & Ganem, B. (1994) *Biochemistry 33*, 3994−4000.
Casey, P. J., Graziano, M. P., & Gilman, A. G. (1989) *Biochemistry 28*, 611−616.
Cleland, W. W. (1995) *Methods Enzymol. 249*, 341−373.
Coleman, D. E., Berghuis, A. M., Lee, E., Lindner, M. E., Gilman, A. G., & Sprang, S. (1994) *Science 265*, 1405−1412.
Cornell, W. D., Ciepak, P., Bayly, C. I., Gould, I. R., Merz, K. M., Jr., Ferguson, D. M., Spellmeyer, D. C., Fox, T., Caldwell, J. W., & Kollman, P. A. (1995) *J. Am. Chem. Soc. 117*, 5179−5197.
Domenighini, M., Pizza, M., & Rappuoli, R (1995) *Handbook of Natural Toxins, Vol. 8, Bacterial Toxins and Virulence Factors in Disease* (Moss, J., Iglenski, B., Vaughan, M., & Tu, A., Eds.) pp 59−80, Dekker, Inc., New York.
Finck-Barbancon, V., & Barbieri, J. T. (1995) *Biochemistry 34*, 1070−1075.
Gilman, A. G. (1987) *Annu. Rev. Biochem. 56*, 615−649.
Graf, R., Codina, J., & Birnbaumer, L. (1992) *Mol. Pharmacol. 42*, 760−764.
Horenstein, B. A., & Schramm, V. L. (1993) *Biochemistry 32*, 9917−9925.
Horenstein, B. A., Parkin, D. W., Estupinan, B., & Schramm, V. L. (1991) *Biochemistry 30*, 10788−10795.
Katada, T., & Ui, M. (1982) *Proc. Natl. Acad. Sci. U.S.A. 74*, 3129−3133.
Katada, T., Tamura, M., & Ui, M. (1983) *Arch. Biochem. Biophys. 24*, 290−298.
Katada, T., Iiri, T., Takahashi, K., Nishina, H., & Kanaho, Y. (1995) *Handbook of Natural Toxins, Vol. 8, Bacterial Toxins and Virulence Factors in Disease* (Moss, J., Igleshi, B., Vaughan, M., & Tu, A., Eds.) pp 459−489, Dekker, Inc., New York.
Kinoshita, Y., Ruble, J. R., & Jeffrey, G. A. (1981) *Carbohydr. Res. 92*, 1−7.
Kline, P. C., & Schramm, V. L. (1993) *Biochemistry 32*, 13212−13219.
Kline, P. C., & Schramm, V. L. (1995) *Biochemistry 34*, 1153−1162.
McDonald, L., Wainschel, L. A., Oppenheimer, N. J., & Moss, J. (1992) *Biochemistry 31*, 11881−11887.
Melander, L., & Saunders, W. J., Jr. (1980) *Reaction rates of isotopic molecules*, pp 4−55, John Wiley and Sons, New York.
Mentch, F., Parkin, D. W., & Schramm, V. L. (1987) *Biochemistry 26*, 921−930.
Merz, K. M., Jr., & Besler, B. H. (1990) *Quantum Chemistry Program Exchange*, No. 589, Indiana University, Bloomington, IN.
Mixon, M. B., Lee, E., Coleman, D. E., Berghuis, A. M., Gilman, A. G., & Sprang, S. R. (1995) *Science 270*, 954−960.
Moss, J., & Vaughan, M. (1977) *J. Biol. Chem.* 252, 2455−2457.
Moss, J., & Vaughan, M. (1988) *Adv. Enzymol. 61*, 303−379.
Neer, E. J., Pulsifer, L., & Wolf, L. G. (1988) *J. Biol. Chem. 263*, 8996−9000.
Northrop, D. B. (1981) *Annu. Rev. Biochem. 50*, 103−131.
Oppenheimer, N. J. (1978) *J. Biol. Chem. 253*, 4907−4910.
Oppenheimer, N. J., & Tashma, R. (1992) *Biochemistry 31*, 2195 (Abstract).
Parkin, D. W., Mentch, F., Banks, G. A., Horenstein, B. A., & Schramm, V. L. (1991) *Biochemistry 30*, 4586−4594.
Poirier, R. A., Wang, Y., & Westaway, K. C. (1994) *J. Am. Chem. Soc. 116*, 2526−2533.

Quinn, D. M., & Sutton, L. D. (1991) in *Enzyme Mechanism from Isotope Effects* (Cook, P. F., Ed.) pp 73−126, CRC Press, Boca Raton, FL.

Rising, K., & Schramm, V. L. (1994) *J. Am.Chem. Soc. 116*, 6531−6536.

Rising, K., & Schramm, V. L. (1997) *J. Am.Chem. Soc. 119*, 27−37.

Rodgers, J., Femec, D. A., & Schowen, R. L. (1982) *J. Am. Chem. Soc. 104*, 3263−3268.

Rose, I. A. (1980) *Methods Enzymol. 64*, 47−59.

Scheuring, J., & Schramm, V. L. (1995) *J. Am. Chem. Soc. 117*, 12653−12654.

Scheuring, J., & Schramm, V. L. (1997) *Biochemistry 36*, 4526−4534.

Schramm, V. L., Horenstein, B. A., & Kline, P. C. (1994) *J. Biol. Chem. 269*, 18259−18262.

Schröder, S., Buckley, N., Oppenheimer, N. J., & Kollman, P. A. (1992) *J. Am. Chem. Soc. 114*, 8231−8238.

Sims L. B., & Lewis, D. E. (1984) *Isot. Org. Chem. 8*, 161−249.

Sims, L. B., Burton, G. W., & Lewis, D. E. (1977) *Quantum Chemistry Program Exchange*, No. 337, Indiana University, Bloomington, IN.

Tamura, M., Nagimori, K., Murai, S., Yajima, M., Ito, K., Katada, T., Ui, M., & Ishii, S. (1982) *Biochemistry 21*, 5516−5522.

Ui, M. (1984) *Trends Pharmacol. Sci. 5*, 277−279.

Van Ness, B. G., Howard, J. B., & Bodley, J. W. (1980) *J. Biol. Chem. 255*, 10710−10716.

Weiss, P. M., Cook, P. F. Hermes, J. D., & Cleland, W. W. (1987) *Biochemistry 26*, 7378−7384.

West, R. E., Jr., Moss, J., Vaughan, M., Liu, T., & Liu, T.-Y. (1985) *J. Biol. Chem. 260*, 14428−14430.

Wolfenden, R. (1972) *Acc. Chem. Res. 5*, 10−18.

BI970379A